New Description of the Disorder in Zeolite ZSM-48

Raul F. Lobo* and Henk van Koningsveld[†]

Contribution from the Center for Catalytic Science and Technology, Department of Chemical Engineering, University of Delaware, Newark, Delaware 19716, and Laboratory for Applied Organic Chemistry and Catalysis, Delft University of Technology, Julianalaan 136, 2628 BL Delft, The Netherlands

Abstract: A new description of the disorder in ZSM-48 is given. It is shown that ZSM-48 is not a code for one material but for a family of materials consisting of tubular pores. The pores are formed of rolled up honeycomb-like sheets of fused T6-rings (T= tetrahedral), and the pore aperture contains 10 T-atoms. Neighboring pores are related by a zero shift along the pore direction or by a shift of half the repeat distance along the pore direction ($\sim$0.5 $\times$ 8.40 Å). Additional T−T dimers fill spaces between the tubes. Using different degrees of disorder, the X-ray diffraction patterns of a variety of samples of ZSM-48 can be simulated. The present description of the disorder yields calculated diffraction patterns that are in better agreement with experimental patterns than previous descriptions. Unlike previous reports on ZSM-48, it is found that some materials can be highly ordered, others present mostly planar faults, and others still are better described by a two-dimensional (disordered) stacking of tubular pores. The local pore topology is the same in all (disordered) models, and the disorder does not block the pores. Differences in catalytic properties are probably due to differences in crystal morphology and size and to differences in the distribution of aluminum in the framework.

Introduction

ZSM-48 is a high-silica zeolite with a one-dimensional 10-ring pore system. It is a valuable solid-acid catalyst and has been used for a variety of acid-catalyzed hydrocarbon reactions.[1−4] The structure of this zeolite is complex because its framework is highly disordered, leading to sharp and broad features in the X-ray diffraction (XRD) powder pattern.[5] Understanding the structural disorder in a zeolite is a necessary condition to understand its catalytic properties. Disorder may be a disadvantage, as fault planes can, for example, effectively block the pore mouth to incoming molecules. Disorder can also be an advantage if a zeolite can be prepared with different degrees of disorder and if it is possible to tailor its catalytic properties by controlling the disorder.[6]

According to Schlenker et al.,[5] the structure of ZSM-48 is best described as a random intergrowth of two different but structurally related polytypes, hereafter called 48A and 48B, with *Cmcm* and *Imma* symmetry. To form the two polytypes, T12 units (T = tetrahedral atom) are connected into chains and these are connected into layers, as depicted in Figure 1. The two polymorphs are described by two layers with different topologies. Each polytype can be constructed using one type of layer only. The intergrowth between 48A and 48B proposed by Schlenker et al. can easily be obtained without changing the connectivity within the constituent layers, as the connection modes between the two polytypes are equal (Figure 1). The experimental diffraction pattern and the calculated diffraction pattern of a random intergrowth of these two polytypes[5] are reproduced in Figure 2a. The agreement is fairly good. However, there are differences between the calculated and the experimental patterns, which suggest that the original description of the disorder may not capture some important features. For example, the four peaks between $2\Theta = 16-19°$ are absent in the simulations. Moreover, the shoulder at $2\Theta \approx 20°$ and the broad feature at $2\Theta \approx 22°$ are not simulated correctly in the calculated pattern.

In addition, one TEM investigation of ZSM-48[7] does not agree with the fault model of Schlenker. For example, the selected-area diffraction pattern (SADP) along the pore direction (i.e., their *h*,0,*l* projection) shows rows of sharp spots for $h = 3n$ and twin spots/diffuse streaks for $h \neq 3n$ (see Figure 2b). The intensity spots superimposed on the diffuse streaks implicate the presence of large domains of different but structurally related polytypes. The observed diffuse scattering, analogous to what is observed in zeolites beta,[8,9] SSZ-33[10] and SSZ-31,[11] is in

(1) Bhattacharya, D.; Chatterjee, M.; Sivasanker, S. *React. Kinet. Catal. Lett.* **1997**, *60*, 395−403.
(2) Jones, C. W.; Zones, S. I.; Davis, M. E. *Appl. Catal., A* **1999**, *181*, 289−303.
(3) Sastre, G.; Chica, A.; Corma, A. *J. Catal.* **2000**, *195*, 227−236.
(4) Nghiem, V. T.; Sapaly, G.; Meriaudeau, P.; Naccache, C. *Top. Catal.* **2001**, *14*, 131−138.
(5) Schlenker, J. L.; Rohrbaugh, W. J.; Chu, P.; Valyocsik, E. W.; Kokotailo, G. T. *Zeolites* **1985**, *5*, 355−358.
(6) Treacy, M. M. J.; Vaughan, D. E. W.; Strohmaier, K. G.; Newsam, J. M. *Proc. R. Soc. London, Ser. A* **1996**, *452*, 813−840.
(7) Kirkland, A. I.; Millward, G. R.; Carr, S. W.; Edwards, P. P.; Klinowski, J. *ACS Symp. Ser.* **1989**, *398*, 574−586.
(8) Newsam, J. M.; Treacy, M. M. J.; Koetsier, W. T.; Degruyter, C. B. *Proc. R. Soc. London, Ser. A* **1988**, *420*, 375-&.
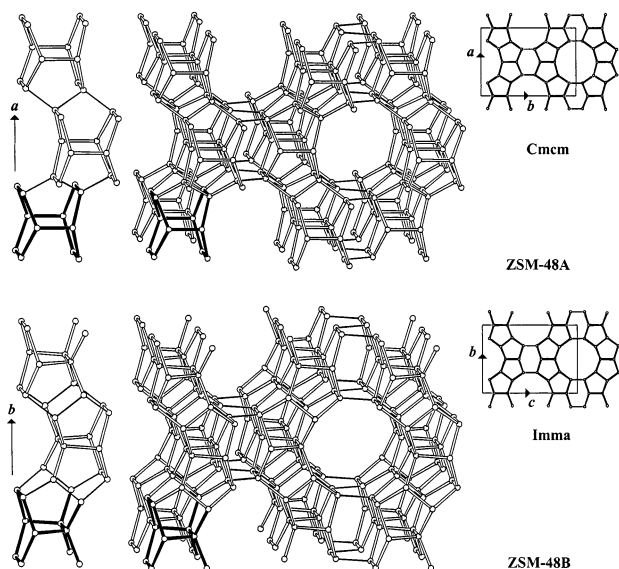
Figure 1. Chain and layers in 48A (top) and 48B (bottom). (Left) T12 units (one in bold), related by a 2-fold screw axis, are connected through T5 rings into a chain. Neighboring chains, related by pure translations along an axis perpendicular to the plane of the paper, are connected into a layer through T4 rings and single T−T connections (middle left part) into an *ac* and *bc* layer in 48A and 48B, respectively. The perpendicular translation is equal to the repeat distance in a crankshaft chain of about 8.4 Å. (Middle) Neighboring *ac* layers in 48A (and *bc* layers in 48B), related by 2-fold axes running parallel to the chain in the layers, are connected through crankshaft chains forming T6 rings. The connecting T−T modes are drawn as single lines. A perspective drawing of the connection mode is shown. (Right) Parallel projection of the unit cell content.

disagreement with the fault model of Schlenker, as faults do not lead to streaks, since the projected potential along the pores does not change with the faults. Thus, further improvements to the existing model of disorder in ZSM-48 are needed.

This paper describes an alternative and fundamentally different characterization of the zeolites ZSM-48 using tubular pores of rolled up T6-ring sheets. Using this description, XRD powder patterns can be simulated which show better agreement with the experimental data than the previous model. The present description also accounts for the TEM results reported by Kirkland et al.[7] It is found that ZSM-48 is not a code for one material but for a family of materials with different degrees of disorder. Different samples, prepared with different structure-directing agents, can have different particle morphologies and dimensions. Particle size differences have an important effect on the appearance of the powder diffraction pattern (in addition to disorder), and these differences can have a measurable effect on catalytic activity and selectivity.

2. Alternative Description of ZSM-48: an Array of Tubular Pores.

In this section, it is shown that ZSM-48 can be conceived as an array of 10-ring pores. To facilitate calculations, two types of layers (built from connecting pores) are used. This perspective will help to characterize the structural disorder.

(9) Higgins, J.; Lapierre, R.; Schlenker, J.; Rohrman, A.; Wood, J.; Kerr, G.; Rohrbaugh, W. *Zeolites* **1988**, *8*, 446−452.
(10) Lobo, R. F.; Pan, M.; Chan, I.; Medrud, R. C.; Zones, S. I.; Crozier, P. A.; Davis, M. E. *J. Phys. Chem.* **1994**, *98*, 12040−12052.
(11) Lobo, R. F.; Tsapatsis, M.; Freyhardt, C. C.; Chan, I.; Chen, C. Y.; Zones, S. I.; Davis, M. E. *J. Am. Chem. Soc.* **1997**, *119*, 3732−3744.
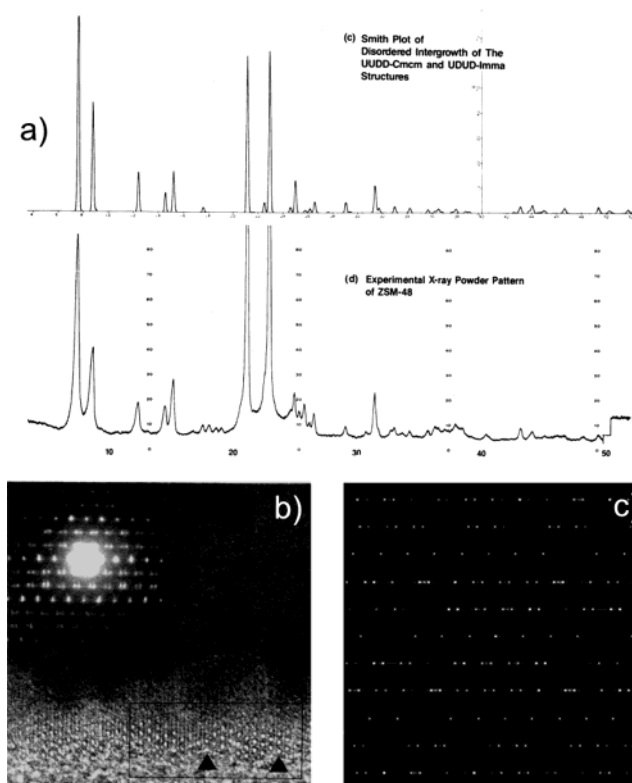
Figure 2. (a) Reproduction of the experimental XRD pattern of ZSM-48 (bottom) and simulated XRD pattern of a random intergrowth of 48A and 48B (top) from ref 5. The inset comments (*c* and *d*) are from the original figure. (Reprinted with permission from Elsevier Science from ref 5, p 357. Copyright (1985).) (b) Reproduction of a high-resolution transmission electron microscopy image and corresponding SADP.[7] Both image and diffraction patterns are taken along the pore axis of the crystal. (Reprinted in part with permission from ref 7. Copyright (1989) American Chemical Society.) (c) Simulated SADP along the pore direction of a ZSM-48 material with $\alpha = 0.2$, $\beta = 0.1$, and $\gamma = 0.8$ (see Section 5).

i. Periodic Building Units. The ZSM-48 polytypes can be built using the crankshaft chain (bold in Figure 3a, left). The repeat unit of the chain consists of four T atoms, and the repeat distance in the chain is ∼8.4 Å. Five crankshaft chains are connected to form a pore with a T10-ring window. The pore wall consists entirely of fused T6 rings. The repeat unit of the tubular pore is a T6-ring band of 20 T atoms (bold in Figure 3a, right). The pores can be considered as being formed of rolled up honeycomb-like sheets of fused T6 rings. Neighboring pores can be connected into layers, hereafter called Periodic Building Units (PerBUs), with or without shifting them with respect to each other along the pore direction *b*. The nonzero shift is equal to half the repeat distance along *b*, which is equal to half the repeat distance in the crankshaft chain (∼0.5 × 8.4 Å). In PerBU1 (Figure 3b), neighboring pores, related by a pure translation along a_1 and a zero shift along *b*, are connected through single crankshaft chains running parallel to *b*. In PerBU2 (Figure 3c), neighboring pores, related by a translation along a_2 and a shift of $^1/_2b$, are connected along a_2 through T4 rings. Close examination of Figure 1 shows that the layers used by Schlenker et al. in the original description of the polytypes are parallel to the (0,1,0) and (0,0,1) in 48A and 48B, respectively, whether the PerBUs are parallel to $(1,\bar{1},0)$ and $(0,1,\bar{1})$ in 48A and 48B (or, equivalently, parallel to (1,1,0) and (0,1,1)).

ii. Connectivity of the Periodic Building Units. The stacking of PerBUs along plane normal *n* requires a lateral shift of the
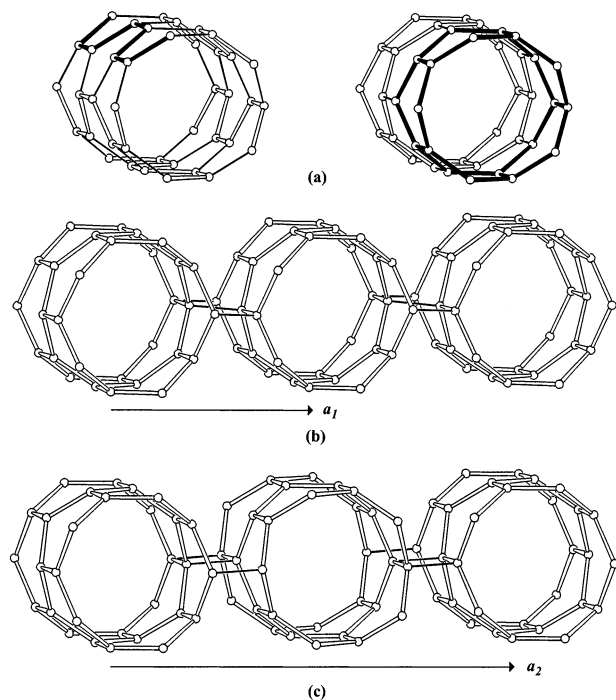
Figure 3. Tubular pores and PerBUs in ZSM-48. In parts b and c, only 1.5 of the repeat unit along the pore axis of the PerBUs is drawn for reasons of clarity. (a) Pore with T10-ring window constructed from five crankshaft chains (left) and from T6-ring bands each consisting of 20 T atoms (right). (b) Tubular pores, related by pure translations along a_1, are connected through single crankshaft chains into PerBU1. (c) Tubular pores, related by a translation along a_2 and a shift of $^1/_2 b$ along the pore axis, are connected through T4 rings into PerBU2.

PerBUs along a (and b) (where n is parallel to $a \times b$ and $|n| = 11.58$ Å; this is done for convenience in the calculations with DIFFaX. The magnitude of n is equal to the height of each PerBU, $|n| = |c| \sin(\beta)$ for polytype **1** (see Table 2)). It is convenient to describe the stacking sequence of the PerBUs along n using the same coordinate system in both PerBUs. Therefore, the unit cell length along the a axis is taken equal to $2 \times |a_1|$ in PerBU1 and equal to $|a_2|$ in PerBU2. For both PerBUs, the lateral shifts along a are then given as $\pm ^1/_6 a$. Direct neighboring PerBUs can be stacked along n in several ways. The lateral shift of the top layer along a and b is the following: (a) $-^1/_6 a$ and zero, denoted as $(-^1/_6, 0)$; (b) $^1/_6 a$ and zero, denoted as $(^1/_6, 0)$; (c) $-^1/_6 a$ and $^1/_2 b$, denoted as $(-^1/_6, ^1/_2)$; and (d) $^1/_6 a$ and $^1/_2 b$, denoted as $(^1/_6, ^1/_2)$, as illustrated in Figure 4 for the connection modes a and c between PerBU1s and for the connection modes b and d between PerBU2s. The PerBUs are connected through crankshaft chains or T4 rings, depending on whether the shift along b between direct neighboring pores is zero or $^1/_2 b$, respectively. The positions of the bridging oxygen atoms between the PerBUs are hardly influenced by whether the PerBUs are connected through T4 rings or through crankshaft chains. This is important because this allows the formation of stacking faults between layers with only minor energetic penalties. Intergrowth of the polytypes is achieved without changing the T6-ring pore topology. The gaps between the T6-ring pores are filled by T−T dimer units connected through additional T4 rings and crankshaft chains. Intergrowth introduces differences in the connections of dimers in the "empty" spaces.

Once the distribution of the lateral shifts between the PerBUs along n is known, the three-dimensional framework is defined.

Examples of the connection modes (a) and (c):

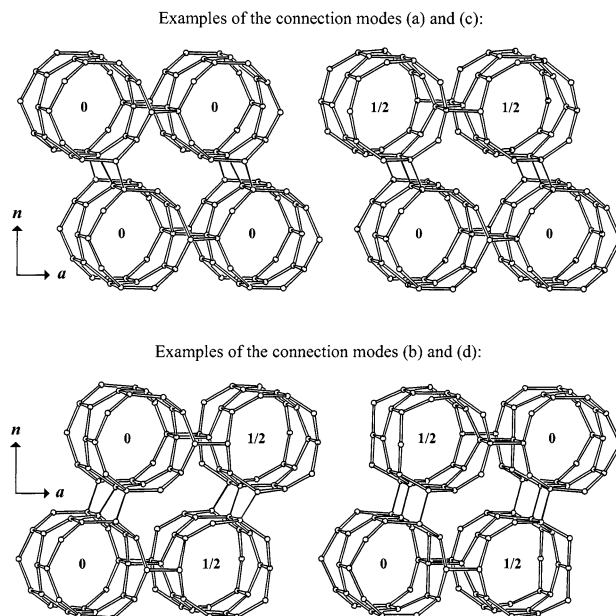Examples of the connection modes (b) and (d):

Figure 4. Illustration of connection modes a and c between PerBU1s (top) and the connection modes b and d between PerBU2s (bottom). The number in the pore gives the fractional shift of the pore along the pore axis b.

Polytype 48A is obtained when neighboring PerBU1s are recurrently stacked along n with lateral shifts of $-^1/_6 a$ and no shift along b (connection mode a). Polytype 48B is obtained when neighboring PerBU2s are recurrently stacked along n with lateral shifts of $-^1/_6 a$ and $^1/_2 b$ (connection mode c).

3. Simplest Polytypes in the ZSM-48 Family of Frameworks

The systematic stacking of PerBU1 and PerBU2 using the connection modes described above gives rise to a series of nine simplest ordered polytypes (Table 1 and Figure 5). For example, polytype **1** (identical to 48A) is generated by stacking PerBU1 using the $(-^1/_6, 0)$ connection mode; polytype **5** is generated by stacking PerBU2 using the $(-^1/_6, 0)$ and the $(^1/_6, 0)$ connection modes sequentially; polytype **8** is generated by stacking alternatively PerBU1 and PerBU2 through a $(-^1/_6, 0)$ connection mode. Polytypes **1** to **4** are generated from PerBU1, **5** to **7** from PerBU2, and **8** and **9** from alternating PerBU1 and PerBU2. To the best of our knowledge, none of these polytypes has been observed yet as a pure phase material. Table 1 provides the symmetries (using the standard setting) and unit cell dimensions of these polytypes, and Figure 5 illustrates the structures of four of them (a complete version of Figure 5 will be presented in the "Catalog of Disorder in Zeolite Frameworks"[12]). The atomic positions have been optimized using the Cerius[2] (ref 13) implementation of DLS-76, and in all cases, reasonable agreement values are obtained.

4. Characterization and Experimental XRD Patterns of ZSM-48 Materials

ZSM-48 is not a code for one material but for a family of materials with similar but not identical XRD patterns. This is evident by inspection of the XRD patterns of the three samples

(12) Giess, H.; Koningsveld, H. v. Catalog of Disorder in Zeolite Frameworks. http://www.iza-structure.org/databases/ (accessed 2002), last update August 2002.

(13) *Cerius*[2], 3.8 edition; Molecular Simulations Inc.; 1998.

Table 1. Simplest Ordered Polytypes of ZSM-48 Described in the Standard Setting of the Space Group

Name	Descriptor[1]	Connection Modes[2]	Space Group	a	b (Å)	c	β (°)
			PerBU1				
1(48A)	○ ○ ○ ○ ○ ○ ○ ○ ○	$(-\frac{1}{6}, 0;$ $-\frac{1}{6}, 0;$ $-\frac{1}{6}, 0; ...)$	Cmcm	14.24	20.14	8.4	-
2	○ ○ ○ ○ ○ ○ ○ ○ ○	$(-\frac{1}{6}, 0;$ $+\frac{1}{6}, 0;$ $-\frac{1}{6}, 0; ...)$	Pmmn	8.4	23.26	12.33	-
3	○ ○ ○ ● ● ● ○ ○ ○	$(-\frac{1}{6}, \frac{1}{2};$ $-\frac{1}{6}, \frac{1}{2};$ $-\frac{1}{6}, \frac{1}{2}; ...)$	C2/m	24.66	8.4	12.33	109.47
4	○ ○ ○ ● ● ● ○ ○ ○	$(-\frac{1}{6}, \frac{1}{2};$ $+\frac{1}{6}, \frac{1}{2};$ $-\frac{1}{6}, \frac{1}{2}; ...)$	Pmma	8.4	23.26	12.33	-
			PerBU2				
3[3]	○ ● ○ ○ ● ○ ○ ● ○	$(-\frac{1}{6}, 0;$ $-\frac{1}{6}, 0;$ $-\frac{1}{6}, 0; ...)$	C2/m	24.66	8.4	12.33	109.47
5	○ ● ○ ○ ● ○ ○ ● ○	$(-\frac{1}{6}, 0;$ $+\frac{1}{6}, 0;$ $-\frac{1}{6}, 0; ...)$	Cmcm	8.4	24.66	23.25	-
6(48B)	○ ● ○ ● ○ ● ○ ● ○	$(-\frac{1}{6}, \frac{1}{2};$ $-\frac{1}{6}, \frac{1}{2};$ $-\frac{1}{6}, \frac{1}{2}; ...)$	Imma	8.4	14.24	20.14	-
7	○ ● ○ ● ○ ● ○ ● ○	$(-\frac{1}{6}, \frac{1}{2};$ $+\frac{1}{6}, \frac{1}{2};$ $-\frac{1}{6}, \frac{1}{2}; ...)$	Cmcm	8.4	24.66	23.25	-
			PerBU1 and PerBU2				
8	○ ○ ○ ○ ● ○ ○ ○ ○	$(-\frac{1}{6}, 0;$ $-\frac{1}{6}, 0;$ $-\frac{1}{6}, 0; ...)$	P2₁/m	24.66	8.4	24.66	109.47
9	○ ○ ○ ○ ● ○ ○ ○ ○	$(-\frac{1}{6}, 0;$ $+\frac{1}{6}, 0;$ $-\frac{1}{6}, 0; ...)$	Pmm2	8.4	23.26	24.66	

[1] Empty (○) and filled (●) circles depict pores that are related by translations of 0.5 × 8.4 Å along the pore direction. [2] The connection modes refer to the displacement along *a* and *b* between consecutive PerBUs (*a* = 24.66 Å and *b* = 8.4 Å). See Figure 4 and text for details. [3] This polytype built from PerBU2 is identical to polytype **3** built from PerBU1.

of ZSM-48 plotted in Figure 6 (top traces). The samples were provided by A. Kuperman (ChevronTexaco Energy Research and Tech. Co.) and have been prepared using three different structure-directing agents. All three samples are highly siliceous materials and have rather distinct morphologies.

Scanning and transmission electron micrographs (not shown) reveal major differences in the particle morphologies and dimensions of the three samples. Sample A consists of individual crystals of ZSM-48. The individual needlelike crystals are ∼20 nm in diameter (as shown by TEM) and about 0.5 μm in length. The particles of sample B (about 4−8 μm long, ∼0.5 μm in diameter) are formed as bundles of long and very narrow crystals, similar to the ones reported by Kirkland et al.[7] From TEM micrographs, a crystal diameter of ∼30 nm is estimated for the narrow crystals. Finally, sample C is formed as needlelike particles of about 3 μm long and 0.5 μm in diameter. Each particle is formed as a small group of long crystals aligned along the particle axis. Each crystal is ∼0.1 μm in diameter.

The main features of the diffraction patterns of all three samples shown in Figure 6 are similar. However, samples A and B have broad peaks partly due to crystal size (needles of less than 50 nm in diameter) and are similar but not identical. For instance, sample A has three small peaks at $2\Theta = 11.6°$,

16.9°, and 17.6°, which are much weaker in sample B. The broad peak at $2\Theta = 25°$ in sample B is shifted to $2\Theta = 24.4°$ in sample A. Sample C has mostly sharp peaks but has several peaks that are not observed in the other two samples and resembles closely the XRD pattern reported in ref 5 (Figure 2a). Note that the peaks at $2\Theta = 11°$ and 13.2°, the four peaks between $2\Theta = 16-20°$, the broad peak at $2\Theta = 21.7°$, and several others in sample C are absent in samples A and B. The alterations in XRD patterns are presumably due to differences in the stackings of the PerBUs in these samples. The XRD pattern of sample C suffers from the effects of preferred orientation. These effects have been minimized by carefully crushing the sample before measurement, but some preferred orientation may still remain reducing the observed relative intensity of the $(0,k,0)$ peaks (e.g., the peak at $2\Theta = 21°$).

Figure 7 compares the calculated XRD patterns of the nine simplest polytypes.[13] These polytypes can be subdivided into two groups: those that can be set into monoclinic unit cells (**1**, **3**, **6**, and **8**; see Table 2) and those with orthorhombic unit cells (**2**, **4**, **5**, **7**, and **9**). This subdivision has been made because the XRD patterns within each group have many similarities. In particular, at a low angle the monoclinic polytypes show two
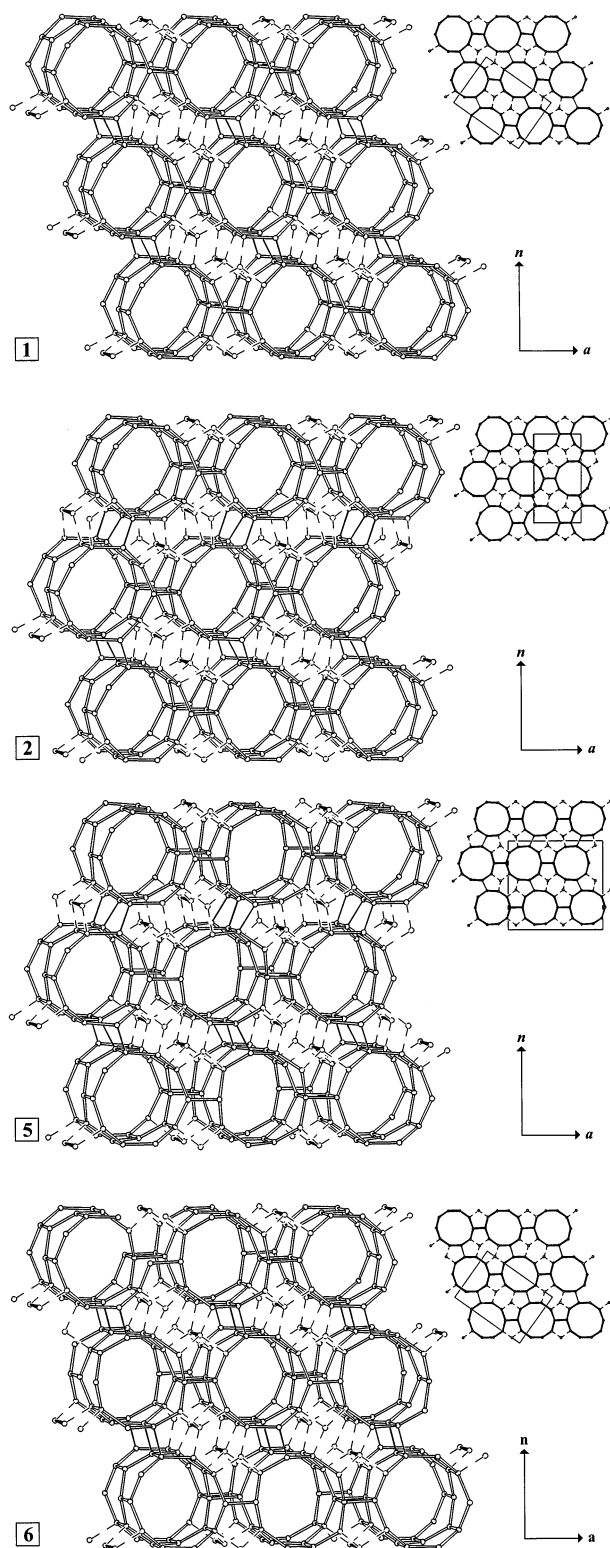
Figure 5. Perspective drawing (left) and parallel projection along the pore axis of the unit cell in standard setting (top right) of the periodic polytypes **1**, **2**, **5**, and **6** in the ZSM-48 family (cf. Table 1). In the simulations (cf. Table 2), the "unit cell" is defined by *a*, *b*, and *n* (bottom right). The *a* axis is in the plane of the PerBU and perpendicular to the pore axis, *b* is parallel to the pore axis, and *n* is parallel to *a* × *b*. Connecting T−T modes between PerBUs are drawn as single lines, and the connections to the space-filling T−T dimers (in heavy bold) are striped.

peaks at $2\Theta = 7.6°$ and $8.8°$, and the orthorhombic polytypes show three peaks at $2\Theta = 7.15°$, $7.6°$, and $8.1°$. The experi-
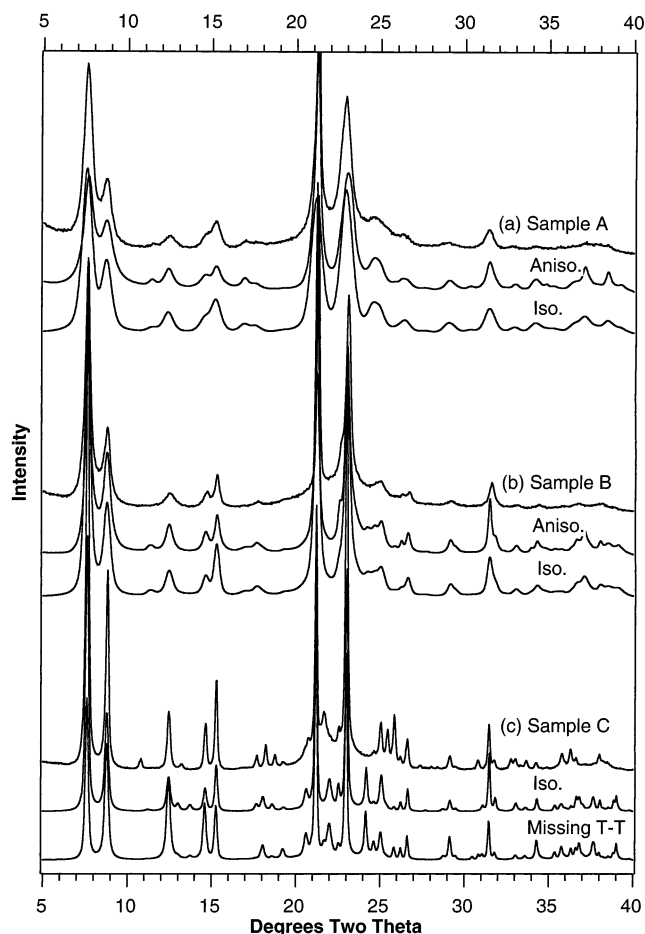
Figure 6. Experimental and calculated XRD patterns of three samples of ZSM-48 (Cu Kα₁ radiation). (a) Comparison of the XRD pattern of sample A (top trace) with the calculated XRD pattern of polytype **6** ($\alpha = 0$, $\beta = 0$, $\gamma = 1$) using a pseudo-Voigt broadening function (bottom trace), and the XRD pattern of polytype **6** using anisotropic broadening (middle trace). The pseudo-Voigt peak shape was calculated with $w = 0.5$ ($u = 0.2$, $v = -0.18$, and $\gamma = 0.6$). For the anisotropic broadening, the crystal dimensions along *a*, *b*, and *c* are 20, 80, and 20 nm respectively. (b) Comparison of the XRD pattern of sample B (upper trace) with the calculated XRD pattern of a faulted structure with $\alpha = 0.2$, $\beta = 0.1$, and $\gamma = 0.8$ using a pseudo-Voigt broadening function ($w = 0.15$, $u = 0.2$, $v = -0.18$, and $\gamma = 0.6$) (bottom trace). Anisotropy of the crystals is also included in the middle trace calculated using crystal dimensions along *a*, *b*, and *c* of 90, 300, and 90 nm respectively. (c) Comparison of the XRD pattern of sample C (upper trace) with the calculated XRD pattern of a faulted structure with $\alpha = 0.8$, $\beta = 0.05$ and $\gamma = 0.05$ (middle trace). A pseudo-Voigt peak shape is used ($w = 0.05$, $u = 0.2$, $v = -0.18$, and $\gamma = 0.6$). The effect of anisotropic broadening seems to be small compared to the those of the other two samples and was not used. In the bottom trace, the XRD pattern is calculated using the same fault probabilities ($\alpha = 0.8$, $\beta = 0.05$, and $\gamma = 0.05$) but with zero occupation factor for the T−T dimers (see section 6). Better agreement with experimental findings is observed in the region $2\Theta = 25-27°$. The XRD patterns were measured using a Siemens D5000 powder diffractometer in Bragg−Brentano geometry using the step scan mode (steps of 0.04°) in a flat sample holder.

mental XRD patterns always show only two peaks at 7.6 and 8.8°, so at the outset it is concluded that ZSM-48 materials more closely resemble the monoclinic polytypes **1**, **3**, **6**, and **8**. Comparison of the monoclinic polytypes with the experimental XRDs shows that all of them have many peaks that coincide with the peaks in the experimental patterns, but at the same time, all have peaks that are not present in the experimental pattern. ZSM-48 materials are faulted, and this feature needs to be included in the simulation of XRD patterns.
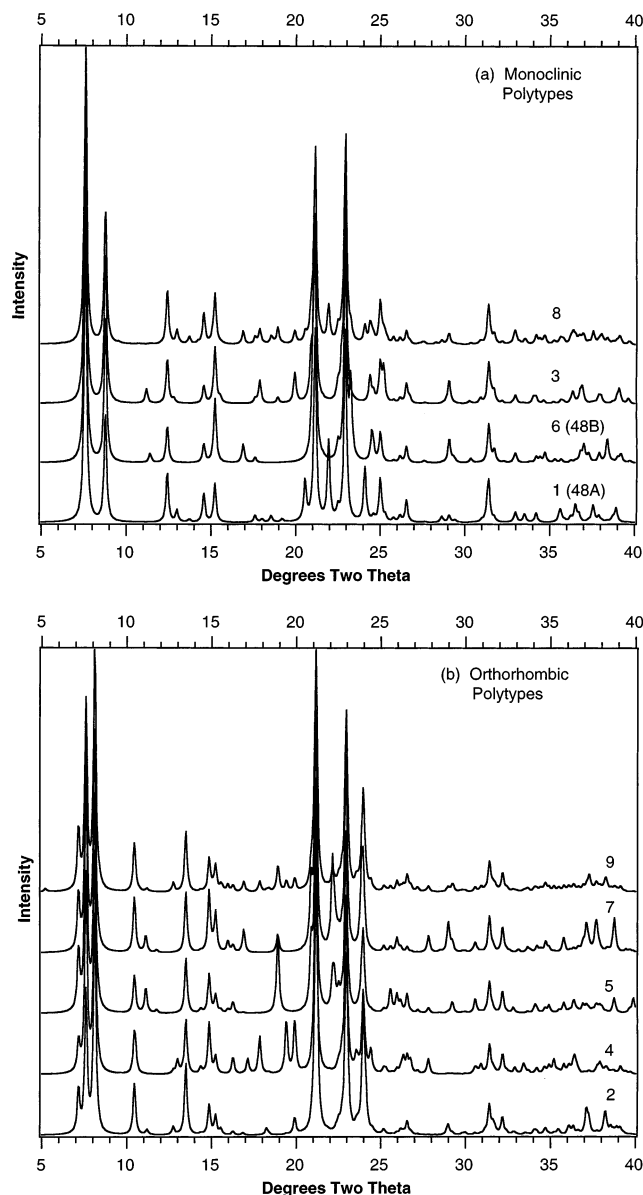
Figure 7. XRD patterns of the simplest polytypes of ZSM-48. (a) Monoclinic polytypes and (b) orthorhombic polytypes. The numbers identify the polytypes according to Table 1. Compare to the experimental XRD patterns in Figure 6. Patterns calculated using Cerius[2] (Cu Kα radiation).[13]

5. Simulation of XRD Patterns of the Faulted Structures

The diffraction patterns of the faulted structures are simulated using the program DIFFaX.[14] For the purpose of these simulations, three distinct fault probabilities will be defined:

(a) Alpha (α) determines the fraction of PerBU1 that forms a particular intergrowth. That is, α is the probability that, after a particular layer i, the next layer is PerBU1. $(1 - α)$ then determines the fraction of PerBU2 that forms the structure.

(b) Beta (β) defines the probability of changing the fault direction. This means that, if a series of PerBUs have been stacked following the $(-^1/_6, 0)$ or the $(-^1/_6, ^1/_2)$ connection modes, the next layer will be stacked in the other direction (i.e., the $^1/_6, 0$ or the $^1/_6, ^1/_2$) with a probability equal to β. Thus, for β = 0, one of the monoclinic polytypes will be obtained, and

for β = 1, one of the orthorhombic polytypes will be obtained (Table 2).

(c) Gamma (γ) defines the probability that the next layer will be stacked following the $(\pm^1/_6, ^1/_2)$ connection mode. This implies a translation of $^1/_2$ b along the pore direction. Thus, if γ = 0, polytypes **1**, **2**, **3**, **5**, **8**, and **9** are obtained, and if γ = 1, polytypes **3**, **4**, and **6** are obtained.

The parameters α, β, and γ are independent of each other and can have values in the range 0−1. Table 2 presents the values of α, β, and γ needed to describe each of the simplest polytypes. The XRD pattern from one polytype changes smoothly to the pattern from another polytype by changing one of the parameters (α, β, or γ) while keeping the others constant. As an example, the effect of changing β while keeping α = 1 and γ = 0 is shown in Figure 8. These materials are built of PerBU1 only, and the XRD pattern changes smoothly from the one of polytype **1** to the one of polytype **2**.

A large number of simulations with many combinations of faulting probabilities have been carried out to investigate how the XRD pattern changes as α, β, and γ change. In general, even small values of β give rise to a pronounced broadening of the XRD peaks (as in Figure 8). In contrast, changes in α and γ modify the intensities but have relatively little effect on peak broadening. This indicates that sample C must have a small value of β (0 < β < 0.1), since it only contains sharp peaks. Calculations of the SADP along the pore direction show that the observations of Kirkland[7] (i.e., rows of sharp spots for $h = 3n$ and diffuse streaks for $h \neq 3n$, Figure 2b) are only reproduced when β ≠ 0.

i. Sample A. Figure 6a shows a comparison of the XRD pattern of sample A with the calculated XRD pattern of polytype **6** (α = 0, β = 0, γ = 1). The diffraction pattern calculated by DIFFaX has been substantially broadened using a pseudo-Voigt function with $w = 0.5$ ($u = 0.2$, $v = -0.18$, and γ = 0.6; lower trace in Figure 6a). The broadening of the XRD peaks is due to the very small size of the crystals (needles of ~20 nm), and very good agreement with experimental findings is obtained without recourse to faulting. This is in agreement with the absence of faulting observed in several preliminary low-magnification high-resolution TEM images of these particles along the pores.[15] The particles are highly anisotropic, with the long particle axis along the b direction (i.e., the pore direction), and the correct fwhm of the 0,2,0 reflection at 2Θ = 21.1° is captured correctly when anisotropic broadening of the pattern is introduced (Figure 6a, middle trace). Although the data does not rule out the presence of faults in this sample, any disorder is infrequent and possibly does not occur within most crystallites, given the very small size of the crystals. Therefore, the structure of sample A greatly resembles the structure of pure 48B (polytype **6**).

ii. Sample B. Sample B has sharper peaks than sample A with different relative intensities in some of the peaks. It has not been possible to accurately simulate the XRD pattern of sample B using any of the pure polytypes listed in Table 1. This characteristic is an indication that sample B has more frequent faults than sample A. To simulate the XRD pattern of sample B, it is necessary to include twinning (β ≠ 0), to combine PerBU1 and PerBU2 (0 < α < 1) and to apply shifts along b (0 < γ < 1) as well. In Figure 6b, the XRD pattern of sample

(14) Treacy, M. M. J.; Newsam, J. M.; Deem, M. W. *Proc. R. Soc. London, Ser. A* **1991**, *433*, 499−520.

(15) Lobo, R. F.; Kooyman, P.; Koningsveld, H. v. In preparation.

Table 2. Fault Probabilities in the Simplest Ordered Polytypes of ZSM-48[3]

Name	Descriptor[1]	Space Group	c (Å)	β (°)	α	β	γ
			PerBU1				
1(48A)	○○○ / ○○○ / ○○○	P2/m	12.33	109.47	1	0	0
2	○○○ / ○○○ / ○○○	Pnmm	23.256	-	1	1	0
3	○○○ / ●●● / ○○○	C2/m	12.33	109.47	1	0	1
4	○○○ / ●●● / ○○○	Pcmm	23.256	-	1	1	1
			PerBU2				
3	○●○ / ○●○ / ○●○	C2/m	12.33	109.47	0	0	0
5	○●○ / ○●○ / ○●○	Ccmm	23.256	-	0	1	0
6(48B)	○●○ / ●○● / ○●○	B2/m	24.66	109.47	0	0	1
7	○●○ / ●○● / ○●○	Ccmm	23.256	-	0	1	1
			PerBU1 and PerBU2				
8	○○○ / ○●○ / ○○○	P2$_1$/m	24.66	109.47	$1/2$[2]	0	0
9	○○○ / ○●○ / ○○○	P2mm	23.256	-	$1/2$[2]	1	0

[1] Empty (○) and filled (●) circles depict pores that are related by translations of ~0.5 × 8.4 Å along the pore direction. [2] In this case, the distributions of PerBU1 and PerBU2 are correlated and are not described precisely by a probability α. PerBU1 and PerBU2 alternate one after the other. [3] The polytypes are described using the PerBUs to define the *ab* plane leading to nonstandard space group settings. In all cases, $a = 24.66$ Å and $b = 8.4$ Å

B (upper trace) and a simulated pattern (using $\alpha = 0.2$, $\beta = 0.1$, and $\gamma = 0.8$ in the lower trace) are given. They show very good agreement when compared. In this case, it has also been necessary to broaden the XRD pattern with the pseudo-Voigt function but now using a smaller value of $w = 0.15$ ($u = 0.2$, $v = -0.18$, and $\gamma = 0.6$). The middle trace in Figure 6b shows the improvement in agreement obtained when crystal anisotropy is introduced into the calculated XRD pattern.

Figure 2c shows the simulated SADP of a sample with $\alpha = 0.2$, $\beta = 0.1$, and $\gamma = 0.8$. It compares well to the SADP reported by Kirkland[7] (see Figure 2b).

Once the XRD pattern has been (anisotropically) broadened to account for the extreme aspect ratio of the particles, the general features of the pattern do not change appreciably for values of α and β that are within ~0.05 of the values reported for sample B. Thus, the values of $\alpha = 0.2$, $\beta = 0.1$, and $\gamma = 0.8$ are only approximate, and materials with larger crystal habits have to be prepared before more accurate numbers can be determined. Sample B can be described as a faulted form of polytype **6** material.

iii. Sample C. Many aspects of the XRD pattern of sample C resemble the XRD pattern of polytype **1**. However, there are several missing peaks in the pattern of sample C, and this

material may also be faulted. Figure 6c compares the experimental XRD pattern of sample C (upper trace) with a simulated one using $\alpha = 0.8$, $\beta = 0.05$, and $\gamma = 0.05$ (middle trace). The pattern calculated with these values shows the closest agreement to the experiment pattern that has been found. There is better agreement between these two patterns than with that of the pure polytype **1**, but there remain several sections with poor agreement. In particular, the peak at $2\Theta = 13.8$ is absent in the experimental pattern, the position of the peaks at $2\Theta \approx 22°$ do not match, and the peak at $2\Theta = 24°$ in the calculated pattern is absent in the experimental one. Thus, it is preliminarily concluded that not only, on average, sample C resembles more closely polytype **1** than the other polytypes but also that the disorder in this sample is not captured correctly by the models described here. It is very likely that this is due to disorder within the layers as discussed below.

6. Disorder within the Layers

The major limitation of the model reported so far is that it assumes that ZSM-48 is built of PerBUs with perfect two-dimensional periodicity. This may be an unrealistic assumption, and more plausibly, there may be also disorder within the layers. This means that the actual layers in ZSM-48 are very probably
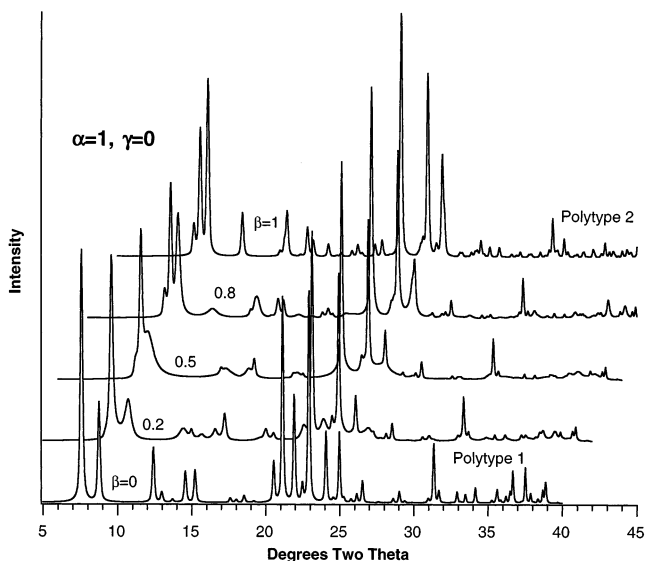
Figure 8. Simulated XRD patterns (DIFFaX,[14] Cu Kα radiation) depicting the effect of changing the fault probability β while keeping $\alpha = 1$ and $\gamma = 0$, i.e., going from monoclinic polytype **1** to orthorhombic polytype **2**. Note that the calculated XRD patterns of the simplest polytypes using DIFFaX are very similar to the ones calculated with Cerius[2].[13] The differences arise mostly from changes in peak broadening which are calculated differently in each program.
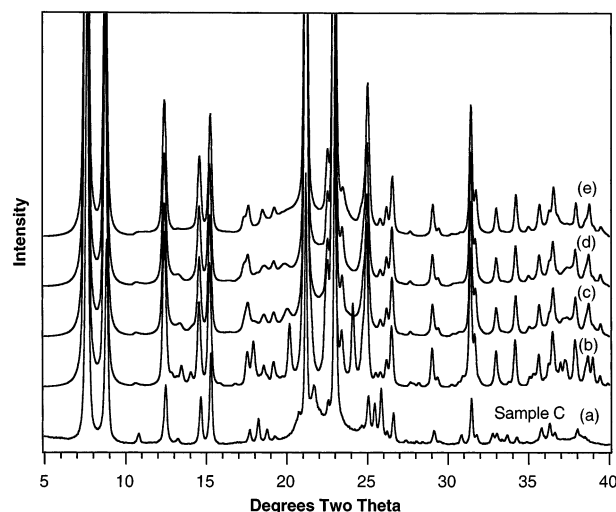

Figure 9. Comparison of the experimental XRD pattern of sample C (trace a) with simulated patterns calculated using a long "disordered" unit cell of 20 pores and different degrees of disorder in the stacking (see text). (b) Trace is obtained using connection mode 1 only. (c) Trace is calculated stacking the layers following connection mode 1 with 55% probability and connection modes 2, 3, and 4 with 15% probability. (d) Trace is a simulated XRD using a probability of 25% for each connection mode (i.e., completely random stacking). (e) Top trace depicts the simulated XRD using the disordered layer but using now eight (instead of four) connection modes (see text).

combinations of the two types of "ideal" layers used to simulate the faulting, and so, ZSM-48 should probably be considered as consisting of a disordered stacking of the tubular pores (rods) described in section 2. This is similar to the description of disorder of the rods in the dodecasil family and in some samples of mordenite, as discussed by Daniels,[16] and Cambel and Cheetham,[17] respectively. In other words, in ZSM-48, there might be two-dimensional disorder and the model presented here is an approximation of the actual disorder in real materials.

The presence of disorder within the layers was explored in sample C. It is possible to approximate the effect of disorder within the layers using DIFFaX.[18] This can be done using a unit cell that contains many T10-ring pores, some of which are translated along the pore direction. A cell containing twenty T10-ring pores has been used: the first six are all stacked without translation along *b*; the next five are translated $^1/_2 b$; the following four are not; and finally, the last five are also translated $^1/_2 \boldsymbol{b}$. The layer contains 1560 atoms with $a = 246$ Å. This layer has been used because it seems, from the previous section, that PerBU1 is the main component of sample C.

The layer can be stacked following the same connection modes that were described for PerBU1 and PerBU2 in section 2. However, it is clear that in this case there are many more possibilities. For example, the layer can be stacked following the $(-^1/_6, 0)$ connection mode plus a translation along *a* of 1 pore diameter (12.33 Å), or 2 pore diameters, or 3, and so forth up to 20. The same is true for each of the other three connection modes. To simplify the scope of the computations, calculations were performed using the following four connection modes only (note that these connection modes are different from the ones described in section 2): (1) $(-^1/_6, 0)$; (2) $(-^1/_6, ^1/_2)$ plus a translation of one pore along *a*; (3) $(-^1/_6, 0)$ plus a translation

of 10 pores along *a*; and (4) $(-^1/_6, ^1/_2)$ plus a translation of 15 pores along *a*.

Figure 9 shows the calculated XRD patterns for materials constructed following these four connection modes with different probabilities. Trace a is the experimental XRD pattern of sample C. Trace b shows the result of using connection mode 1 only. Trace c shows the effect of having the four connection modes with 55%, 15%, 15%, and 15% probabilities, respectively. A clear improvement in the agreement with experimental findings is observed. The calculated sharp peak at $2\Theta = 24°$ is not observed any more, and evidence for small peaks at $2\Theta = 11°$ and 13.2° is also observed. Trace d shows the XRD pattern of a material built using the four connection modes with equal probability (25%). Several further improvements are observed such as the reduction in intensity of the peak at $2\Theta \approx 20°$ and better agreement in the region $2\Theta = 35-40°$. Finally, trace e shows the XRD pattern obtained using four additional connection modes (with translations of 2, 6, 7, and 17 pores along *a*, all with equal probability), to determine the effect of even more disorder. The simulated XRD (Figure 9, top trace) does show some areas of further agreement with experimental findings, but in some other areas, the agreement decreases. Improvement is observed for the peak at $2\Theta = 20°$, which is not observed any more, as well as for the peak at $2\Theta = 23.5°$, which shows a decreased intensity. On the other hand, the small peaks at $2\Theta = 11°$ and 13.2° are barely detectable in the calculated XRD pattern, whereas they are clearly present in the experimental XRD pattern.

The point of these simulations is to illustrate that some of the disagreement between the calculated XRD pattern of sample C and the experimental pattern in section 5 can be accounted for qualitatively by disorder within the layers. It is unreasonable to suppose that the XRD pattern can be reproduced using just one unit cell with 20 "disordered" pores. More or less disorder within the layer of pores or correlations in the way the pores

(16) Daniels, P. *J. Appl. Crystallogr.* **1998**, *31*, 559−569.
(17) Cambel, B. J.; Cheetham, A. K. *J. Phys. Chem. B* **2002**, *106*, 57−62.
(18) Braunbarth, C.; Hillhouse, H. W.; Tsapatsis, M.; Burton, A.; Lobo, R. F.; Jacubinas, R. M.; Kuznicki, S. M. *Chem. Mater.* **2000**, *12*, 1857−1865.

are related to their neighbors [6] (e.g., the presence of domains of orthorhombic symmetry) may appreciably change the calculated XRD pattern. The calculations do show that the most likely reason for the disagreement between the calculated XRD pattern and the experimental pattern in Figure 6c is disorder within the layers.

A major point of concern is the region between $2\Theta = 25-27°$, which shows in sample C an intensity distribution not matched by any of the pure monoclinic polytypes (Figure 7). This may suggest that there are still other aspects of the disorder that are not captured by the two-dimensional disorder model. Tentatively, it is suggested that perhaps the T$-$T dimers depicted in Figure 4 are often absent in some samples of ZSM-48. These T$-$T dimers are not part of the T10-ring pore and kinetically may not be completely filled during crystal growth leading to T vacancies in the structure. In Figure 6c (lower trace), the XRD pattern calculated using $\alpha = 0.8$, $\beta = 0.05$, and $\gamma = 0.05$ is plotted using an occupation factor of zero for the T$-$T dimers (the middle trace shows the XRD pattern with full occupation). The trends are actually in the right direction, and in the region for $2\Theta = 25-27$, there is more agreement with the experimental findings when these T atoms are absent.

7. Summary and Conclusions

It has been shown that the existing model of disorder in zeolite ZSM-48 does not account quantitatively for the XRD patterns of samples reported in the open literature and does not explain the qualitative features of reported SADP. A new description of the disorder in the zeolite has been presented on the basis of the stacking of layers composed of T10-ring pores. Two types of ordered layers are described that can be connected following four connection modes. These two layers and connection modes have been used to enumerate nine simplest polytypes.

Three samples of ZSM-48 have been investigated, each showing a distinct XRD pattern and crystal morphology. In sample A, the evidence indicates that the sample is *not* disordered and that peak broadening can be explained satisfactorily by the crystal dimensions and anisotropy of the crystal morphology. Sample A is one of the polytypes described originally by Schlenker (48B) and described here as polytype **6** (with $\alpha = 0$, $\beta = 0$, $\gamma = 1$). The XRD pattern of sample B cannot be simulated using any of the pure polytypes. Sample B is faulted, and the disorder can be explained by the new model presented here. Very good agreement between simulated and experimental XRD patterns can be obtained using fault probabilities of $\alpha = 0.2$, $\beta = 0.1$, and $\gamma = 0.8$ which resembles that of a faulted polytype **6**. The simulated SADP with these parameters is also in qualitative agreement with the SADP reported by Kirkland et al.,[7] for their sample of ZSM-48. In sample C, it was not possible to simulate the XRD pattern satisfactorily using neither of the two types of *ordered* layers described in Section 2. Some aspects of the disorder in this sample are not captured by the model. It appears that the disorder

in this sample is two-dimensional, that is, there is disorder within the layers of pores that form the material. The agreement between experimental and calculated XRD patterns for sample C was improved when disorder within a layer is introduced. The stacking of these layers is also disordered. The agreement, however, seems to improve somewhat by changing the occupation factors of the pore-connecting T$-$T dimers. The agreement with experimental findings is still not quantitative, and further study of this sample is needed to obtain a completely satisfactory description of its structure.

Since the three samples investigated here show qualitatively different degrees of disorder, other samples prepared with different reagents, different structure-directing agents, and different reaction conditions are likely to also have different degrees of disorder. Thus, it is better to think about ZSM-48 as a family of materials built from T10-ring pores formed of rolled-up T6-ring sheets. These T10-ring pores can be organized, following several connection modes where a particular material will have a specific set of connection modes with a certain specific probability.

As a result of the data provided here, a very different view of the ZSM-48 family of materials has emerged. ZSM-48 is not a random intergrowth of 48A and 48B, as proposed by Schlenker et al.[5] In fact, some samples are actually highly ordered, while other samples show different degrees of disorder. The description of the disorder given in this manuscript is a simplified (yet practical) approximation to the types of disorder observed in ZSM-48.

The local pore topology in all our (disordered) models is the same (T10-ring pores of rolled up T6-ring sheets), and the disorder does not block the pores. Therefore, differences in catalytic properties probably are due to differences in sizes and morphologies of the crystals and to differences in the distributions of aluminum in the framework. Unfortunately, the characterization of ZSM-48 samples that is often found in the open literature is poor (e.g., frequently no XRD patterns are given). It is imperative that, in the future, high quality XRD patterns and high-magnification SEM images are provided for all samples of ZSM-48; otherwise the important practical issue of catalytic structure$-$property relationships may never be resolved.